High Energy Density Physics 9 (2013) 528–534

Contents lists available at SciVerse ScienceDirect

High Energy Density Physics

journal homepage: www.elsevier.com/locate/hedp

# Review of the 1st Spectral Line Shapes in Plasmas code comparison workshop

Evgeny Stambulchik

*Faculty of Physics, Weizmann Institute of Science, Rehovot 76100, Israel*

ARTICLE INFO

*Article history:*
Received 2 May 2013
Accepted 2 May 2013
Available online 11 May 2013

*Keywords:*
Spectral line shapes
Stark broadening
Zeeman effect
Numerical methods
Computer simulations

ABSTRACT

A review is given of the first workshop dedicated to the detailed comparison of various approaches to the calculation of spectral line shapes in plasmas. A standardized set of case problems was specified in advance, together with the prescribed atomic data and assumptions to be used. In this brief review, motivations for the case problems chosen are outlined, followed by a discussion of selected results. Plans for the next workshop are discussed in the conclusion.



## 1. Introduction

Line-shape analysis is one of the most important tools for diagnostics of both laboratory and space plasmas [1]. Its reliable implementation requires sufficiently accurate calculations. In the formation of a line shape Stark broadening is the most computationally challenging contribution, with other factors, such as the Zeeman and Doppler effects, further complicating the calculations. Therefore, except for limiting cases, line-shape calculations imply the use of computer codes of varying complexity and requirements of computational resources. There exist several such codes and, necessarily, limits of applicability, accuracy, and in the end, results, differ from one to another. However, studies comparing different computational and analytical methods are almost nonexistent. The 1st Spectral Line Shapes in Plasma (SLSP) code comparison workshop [2] was organized to fill this gap. The organization of the meeting was modeled after the very successful series of NLTE workshops running from the mid 1990's [3] until now [4]. The NLTE workshops were inspired by the Opacity Workshops, initiated in the late 1980's [5], where a detailed comparison of results for a preselected set of standardized case problems was carried out and analyzed.

A general review of the SLSP workshop is presented, focusing on motivation for the case problems chosen, and followed by discussion of selected results.

## 2. Cases

A number of transitions were selected and are presented in Table 1. For each transition results on a grid of electron densities ($n_e$) and temperatures were requested – assuming one temperature for the ions and electrons, i.e., $T = T_e = T_i$. For each case, the atomic and plasma models are specified, and for some cases, there are more than one atomic or plasma model suggested. Here unless specified otherwise, the plasma is assumed to be quasi-neutral, consisting of electrons and a single type of ions. In addition, some cases are further detailed by specifying extra parameters, such as the magnetic field. In total, 184 subcases were defined.

In order to exclude the influence of variance of atomic data on the results, the case definitions also included exact atomic models to be used. That is, provided were a list of the levels to be accounted for, level energies, and matrix elements between them.

### 2.1. Reference cases

1. Hydrogen Lyman-$\alpha$ in an ideal plasma is a classical ion-dynamics test.
2. A relatively high-$n$ line for hydrogen. For the plasma parameters selected, this is a test of the transition for electrons from dynamic to almost static regime.

These cases are not necessarily realistic, but are good for basic comparison and understanding what is wrong/different if there is a significant scatter in the results from the more advanced cases below. There are quite a few sub-cases of these reference cases; however, the

*E-mail address:* Evgeny.Stambulchik@weizmann.ac.il.

1574-1818/$ – see front matter © 2013 Elsevier B.V. All rights reserved.
http://dx.doi.org/10.1016/j.hedp.2013.05.003

**Table 1**
Case definitions.

| ID | Transition(s) | $n_e$ ($cm^{-3}$) | $T$ (eV) | Extra parameters |
|---|---|---|---|---|
| 1 | H Lyman-$\alpha$ | $10^{17}$, $10^{18}$, $10^{19}$ | 1, 10, 100 | – |
| | Model: $\Delta n \neq 0$ interactions ignored (strictly linear Stark effect); no fine structure; ideal plasma (straight path trajectories and infinite Debye length for MD or Holtsmark distribution for analytical models) in three variants: only electrons, only protons, and electrons and protons together. | | | |
| 2 | H Lyman-$\delta$ | $10^{16}$, $10^{17}$, $10^{18}$ | 1, 10, 100 | – |
| | Model: same as above. | | | |
| 3 | H $n = 6 \rightarrow 5$ | $5 \times 10^{15}$, $2 \times 10^{6}$ | 1, 10 | – |
| | Model: $\Delta n \neq 0$ interactions included in three approximations: none, only $n = 5$ and 6 levels interact, and all from $n = 5$ to $n = 7$. Plasma ions: protons. | | | |
| 4 | Be II $3s$–$3p$ | $10^{17}$ | 5, 15, 50 | – |
| | Model: $3s$, $3p$, and $3d$ levels included, no fine structure. Only electron broadening included, in two approximations: straight paths and hyperbolic trajectories. | | | |
| 5 | N V $3s$–$3p$ | $10^{18}$ | 5, 15, 50 | – |
| | Model: same as above. | | | |
| 6 | Ne VIII $3s$–$3p$ | $10^{19}$ | 5, 15, 50 | – |
| | Model: same as above. | | | |
| 7 | Al III $4s$–$4p$ | $10^{18}$ | 2, 4, 8 | – |
| | Model: $4s$, $4p$, and $4d$ levels included, no fine structure. Plasma perturbations in two approximations: only electrons and both electrons and ions (Al III). | | | |
| 8 | Si XIII $n = 3 \rightarrow 1$ | $10^{21}$, $10^{22}$, $10^{23}$ | 300 | – |
| | Model: $n = 1$ and 3 singlet levels only, ignoring $\Delta n \neq 0$ interactions. Plasma ions are protons. | | | |
| 9 | Al XIII Lyman-$\alpha$ | $10^{21}$, $10^{22}$ | 500 | $\omega = 10^{15}$ rad/s, $F = 0$, 1, 2 GV/cm |
| | Model: $n = 1$ and 2 levels in two variants: with and without fine structure. Plasma ions are Al XIII, no electrons. | | | |
| 10 | D Balmer-$\alpha$ | $2 \times 10^{14}$, $10^{15}$ | 1, 5 | $B = 0$, 5, 10 T |
| | Model: with/without fine structure for the lower/higher density, respectively; ideal plasma in two variants: ions are either deuterons or infinitely massive particles. | | | |
| 11 | D Balmer-$\beta$ | $2 \times 10^{14}$, $10^{15}$ | 1, 5 | $B = 0$, 5, 10 T |
| | Model: same as above. | | | |
| 12 | D $n = * \rightarrow 2$ | $10^{15}$, $10^{16}$, $10^{17}$ | 1 | – |
| | Model: fully ionized D plasma, LTE, two variants: only bound–bound transitions included or both bound–bound and free–bound. | | | |
| 13 | H Balmer-$\alpha$ | $10^{18}$ | 1 | – |
| | Model: linear Stark, plasma in two variants: ideal and interacting. Plasma ions: protons. | | | |
| 14 | H Balmer-$\beta$ | $10^{18}$ | 1 | – |
| | Model: same as above. | | | |
| 15a | Ar XVII He-$\beta$ | $5 \times 10^{23}$, $10^{24}$, $2 \times 10^{24}$ | 1000 | – |
| | Model: plasma ions are deuterons with 0.1% of Ar XVII. | | | |
| 15b | Ar XVI He-$\beta^*$ $n = 2$ | $5 \times 10^{23}$, $10^{24}$, $2 \times 10^{24}$ | 1000 | – |
| 15c | Ar XVI He-$\beta^*$ $n = 3$ | $5 \times 10^{23}$, $10^{24}$, $2 \times 10^{24}$ | 1000 | – |
| 15d | Ar XVI He-$\beta^*$ $n = 4$ | $5 \times 10^{23}$, $10^{24}$, $2 \times 10^{24}$ | 1000 | – |
| | Atomic model: with and without the interference term in the electron broadening; plasma model: as above. | | | |

corresponding models are purposefully made simple: 1) we assume an ideal plasma which for the line broadening calculations will mean straight path trajectories and infinite Debye length for molecular dynamics (MD) simulations, or a Holtsmark distribution for analytical approaches and 2) pure linear Stark effect so that interactions between states with $\Delta n \neq 0$ are ignored and no fine structure is included. In order to assess the influence of electrons and ions, which are protons for the reference cases, the broadening was calculated assuming the electrons and protons act separately and together, so that there are three variants in total for each pair of $n_e$ and $T$.

### 2.2. High-n $\Delta n = 1$ transitions

3. Hydrogen $n = 6 \rightarrow n = 5$ transition. This case was calculated using three atomic models: (i) no $\Delta n \neq 0$ coupling accounted for, (ii) $n = 5$ and $n = 6$ states couple, and (iii) $n = 5$, 6, and 7 states included in the Hamiltonian and allowed to mix.

This line is a representative of $n, n' \gg 1, \Delta n \ll n$ class of transitions that includes the radio-frequency lines, which are of great interest for astrophysics. However, due to the computational costs, an $n$ was chosen that is not sufficiently high to be categorized as a radio-frequency transition. Nevertheless, the couplings between states with $\Delta n \neq 0$ were important.

### 2.3. Isolated lines

First, three species from the Li-like $3s$–$3p$ sequence were chosen, for which the divergence between quantum mechanical (QM) calculations and experiments grows with $Z$ [6]:

4. Be II is the first non-neutral species of the sequence.
5. N V – an intermediate $Z$.
6. Ne VIII is about the highest $Z$ for which the $3s$–$3p$ broadening can be reliably measured.

The plasma model for these cases included only electrons, and it was assumed that they move either along straight path trajectories or the more realistic quasi-classical hyperbolic trajectories (due to the Coulomb interaction with the radiator) in order to investigate this effect.

In addition, another isolated line was considered for which quantum effects are not expected to be so significant (i.e., larger matrix elements and cross-sections):

7. Al III $4s$–$4p$. In addition to the width, values of the line shift were compared.

### 2.4. Intermediate case between isolated and degenerate regimes

8. He-like Si XIII $3 \rightarrow 1$ transitions without inter-combination lines. At the lower density, only $1s$–$3p$ (He-$\beta$ proper) is seen, then $1s$–$3d$ and $1s$–$3s$ appear as well, approaching Lyman-$\beta$-like shape at the highest density. Plasma ions are protons.

### 2.5. External fields

9. Al XIII Lyman-$\alpha$ under external harmonic perturbation, e.g., a laser. The functional dependence of the electric field is $F\cos(\omega t)$, with $\omega$ and $F$ given in Table 1. The two plasma densities correspond to laser-dominated and plasma-dominated line

shapes. Two variants of the atomic model were specified: one with and one without fine structure taken into account.
10. Deuterium (D) Balmer-$\alpha$ in the presence of magnetic field, parameters typical for tokamaks. Differences between dynamic and quasi-static ions were investigated.
11. Same for D Balmer-$\beta$.

### 2.6. High-n merging with continuum

12. D Balmer series at $T = 1$ eV and three densities, the lowest one corresponding to tokamak conditions [7] but without the magnetic field. The higher densities are typical for white dwarf photospheres [8].

These calculations are rather advanced, covering broad spectra from discrete levels that start to overlap between themselves and continuum states.

### 2.7. Influence of particle correlations on electric microfields

13. H Balmer-$\alpha$ in two plasma model variants: without interactions between the plasma particles (ideal plasma) and with such interactions.
14. H Balmer-$\beta$. Same as above.

In this set of cases the focus was on analyzing the correlation properties of plasma fields and their effect on line shapes. To this end, a set of statistical properties of the microfields were compared in each calculation case. These are (i) distributions of magnitudes of the "slow" and "fast" components of the total micro-field $\vec{F}(t) = \vec{F}_{\mathrm{e}}(t) + \vec{F}_{\mathrm{i}}(t)$, defined as [9]

$$\vec{F}_{\mathrm{slow}}(\Delta t; t) = \int_{-\Delta t/2}^{\Delta t/2} \vec{F}(t - t')\mathrm{d}t' \tag{1}$$

and

$$\vec{F}_{\mathrm{fast}}(\Delta t; t) = \vec{F}(t) - \vec{F}_{\mathrm{slow}}(\Delta t; t), \tag{2}$$

respectively, and (ii) correlations between directionalities of microfield components [10]

$$C_{\mathrm{ab}}(\tau) = \int \mathrm{d}t\, \vec{\phi}_{\mathrm{a}}(t) \cdot \vec{\phi}_{\mathrm{b}}(t + \tau), \tag{3}$$

where

$$\vec{\phi}_{\mathrm{a}}(t) = \frac{\vec{F}_{\mathrm{a}}(t)}{F_{\mathrm{a}}(t)}, \tag{4}$$

and the indices $a$ and $b$ represent either electrons ($e$) or ions ($i$).

### 2.8. Satellite broadening

15. Ar XVII He-$\beta$ and its Li-like satellites. The argon He-$\beta$ composite spectral feature is observed in inertial confinement fusion implosion core plasmas when a trace amount of argon is added to the deuterium gas fill to diagnose the plasma conditions. This spectral feature is comprised of the $n = 1$ to $n = 3$ line transition in He-like Ar and satellite line transitions in Li-like Ar. It is temperature and density sensitive through the density dependence of the Stark-broadened line shapes and the temperature and density dependence of the atomic level populations. In implosion-core dense plasmas the Stark broadening effect dominates the line shapes. The details of these line shapes and their overlapping, impact the photon-energy dependent emissivity and opacity that, in turn, determine the emergent intensity distribution of the spectral feature and its diagnostic properties [11].

Case 15a corresponds to Ar XVII He-$\beta$ proper, and 15b, c, d to its Ar XVI $n = 2$, $n = 3$, and $n = 4$ spectator satellites, respectively. This was another advanced case (in fact, the most computationally challenging in the workshop program).

## 3. Organization of the workshop and contributions

Following a discussion between future participants, a preliminary set of the test cases was defined in October 2011 and finalized in January 2012. In February, submission of results began, with a deadline set at two weeks prior to the workshop beginning.

20 participants from 9 countries submitted 911 line-shape calculations in total, using 25 different codes (33 including variants). The codes are listed in Table 2. The codes implement a number of different approaches and algorithms. We roughly categorize these in two groups: 1) those employing a variant of the computer simulation modeling [12] and 2) others, labeled in the table as "S" and "O", respectively. Also indicated there are the case(s) for which a code submitted.

The results were submitted in an XML format, designed specifically for this purpose. The data included the spectra calculated (or only width and/or shift, when required), micro-field distributions and correlation functions, estimated accuracy of the calculations, and meta data such as the date of calculation, version, information etc. A special utility, built as a Firefox [13] extension, was developed. The utility provided functions for data upload, verification, plotting, analysis, and comparison with other results. A screen shot of the SLSP utility is given in Fig. 1, where a subset of results submitted for case 3 is shown. In the spirit of the workshop, here and further throughout the paper, the codes are either given dummy labels or not labeled at all. However, the participants of the workshop were able to see the real names.

The workshop commenced with a series of short talks given by the participants, describing their codes and models used. These were followed by "case" sessions devoted to analysis, comparison, and discussion of results, interspersed with a few lectures of common interest given by A. Demura, N. Konjevic, and V. Lisitsa, and concluded with a round-table discussion. For each case session, a coordinator (or two) was appointed in advance, who analyzed the respective results, prepared an overview, and led the discussion. The calculation cases were grouped into the following sessions (with the coordinator names given in parentheses): "Reference" cases (M.Á. González), Isolated lines (S. Sahal-Brechot and M. Dimitrijević), External fields (S. Alexiou and S. Ferri), Field correlations (A. Calisti), Satellite broadening (R. Mancini), High-$n$/continuum merging (C. Iglesias), H-like beyond linear approximation (E. Stambulchik).

## 4. Comparisons

An overall comparison of results is presented in Fig. 2. For each calculation subcase i (determined by a combination of the plasma density, temperature, and extra parameters, see Table 1), and each code, we evaluate and plot ratios between full-width-at-half-maximum (FWHM) value $w_{\mathrm{i}}$ to an average of FWHM of all results submitted for the given subcase:

**Table 2**
A list of the codes participated in the workshop. Type "S" stands for a computer simulation method, "O" for another approach. "+" indicates that results for a given case were submitted.

| Code | Institution | Type | Cases | | | | | | | | | | | | | | |
|---|---|---|---|---|---|---|---|---|---|---|---|---|---|---|---|---|---|
| | | | 1 | 2 | 3 | 4 | 5 | 6 | 7 | 8 | 9 | 10 | 11 | 12 | 13 | 14 | 15 |
| BINGO | CNRS/AMU, France | S | | | | | | | | | | | | | + | + | |
| DARC-GRASP0 | IAPCM, China | O | | | | + | + | + | + | | | | | | | | |
| DM-SIMULATION | U. Valladolid, Spain | S | | | | | | | | | | | | | + | + | |
| ER-SIMULATION | U. Valladolid, Spain | S | + | + | + | | | | | | | | | | + | + | |
| FFM | CNRS/AMU, France | O | | | | | | | | | | + | + | | | | |
| HNG | U. Crete, Greece | S | | + | + | | | | | | | | | | | | |
| HSTRK | U. Crete, Greece | S | + | | | | | | | | | | | | | | |
| LINEAR | U. Crete, Greece | S | | | | | | | | | + | | | | | | |
| MD-SIMU | CNRS/AMU, France | S | | | | | | | | | + | + | + | | | | |
| MELS | LLNL, USA | O | + | + | + | + | + | + | | + | | | | + | | | + |
| MERL | U. Reno, USA | O | + | | | + | + | + | | + | | | | | | | + |
| MERL2 | U. Reno, USA | O | | | | | | | | | | | | | | | + |
| LSNS | AMU, France | S | | | | | | | | | | + | | | | | |
| PPP | CNRS/AMU, France | O | + | + | + | | | | | + | | | | + | | | + |
| PST | U. Crete, Greece | O | | | + | | | | | | | | | | | | |
| QC-FFM | WIS, Israel | O | + | + | + | | | | | | + | + | + | + | | | |
| QUANTSTAT | U. Rostock, Germany | O | + | + | | | | | | | | + | + | | | | |
| QUANTST-MMM | U. Rostock, Germany | O | + | + | | | | | | | | | | | | | |
| SCP | OP-LERMA/AOB, France/Serbia | O | | | | + | + | + | + | | | | | | | | |
| SCRAM | SNL, USA | O | | | | | | | | | | | | + | | | |
| SIMU | WIS, Israel | S | + | + | + | + | + | + | + | + | + | + | + | + | + | + | |
| SIMULATION | U. Valladolid, Spain | S | | | + | + | + | + | | | | + | + | | | | |
| ST | U. Crete, Greece | O | | | + | | | | | | | | | | | | |
| STARCODE | U. Crete, Greece | O | | | | + | + | + | + | | | | | | | | |
| STARK | KIAE, Russia | O | | | | | | | | | | | | | + | + | |

$$R_i \equiv \frac{w_i}{\langle w_i \rangle_{\text{codes}}}. \quad (5)$$

Only subcases with no external electric or magnetic fields were included, since FWHM of a line shape split by an external field is hardly a meaningful measure.

For a majority of the cases, the results show reasonable agreement – defined as not deviating from the average by more than 2 in either direction – indicated by the dashed lines in the figure. However, the scatter of the case-1 results is rather anomalous. One recalls (see Table 1) that these are line-shape calculations of the *simplest* (from the atomic structure point of view) transition, i.e., Ly-$\alpha$. This is in a stark contrast to the case-15 calculations, where the transitions in question are extremely complicated, containing thousands of individual components – yet showing a fair agreement between different contributions. In part, this can be attributed to a lesser number of codes contributed to case 15. However, comparing the results of case 1 (Ly-$\alpha$) and 2 (Ly-$\delta$) exhibits the same trend – the widths of the more complex Ly-$\delta$ transition show significantly less scatter. Furthermore, even the functional dependences of the Ly-$\alpha$ width on the plasma temperature and density, seen in Fig. 3(a) and (b), respectively, are different for different codes. One sees, for example, that in the range of 1–10 eV, some calculations predict that the Ly-$\alpha$ width increases when the plasma temperature increases, while results of others indicate the opposite trend. The dependence on the plasma density of different results varies from the linear $\sim n_e$ to the $\sim n_e^{2/3}$ regime, corresponding, respectively, to the impact- and quasistatic-limit approximations [14].

The other region in Fig. 2 with an anomalously large disagreement between different results corresponds to case 10 (Balmer $\alpha$), i.e., also a $\Delta n \equiv n - n' = 1$ transition (here, $n$ and $n'$ are the principal quantum numbers of the upper and lower levels of the transition,

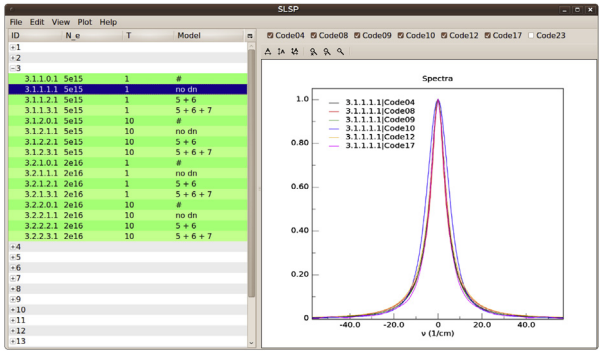


**Fig. 1.** The SLSP utility, built as a Firefox extension, provided a multi-platform, rich graphical user interface.

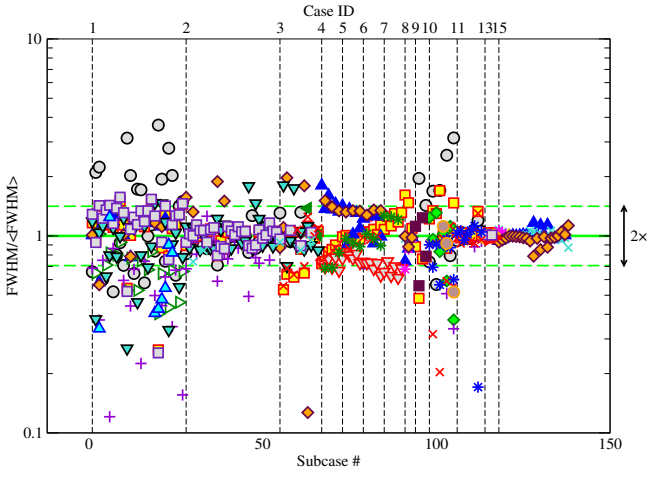


**Fig. 2.** Overall comparison of the workshop results. For each subcase, plotted is a scatter of ratios between different results and an average value. Different symbols correspond to different submissions. Only results of subcases with no external electric or magnetic fields are shown.

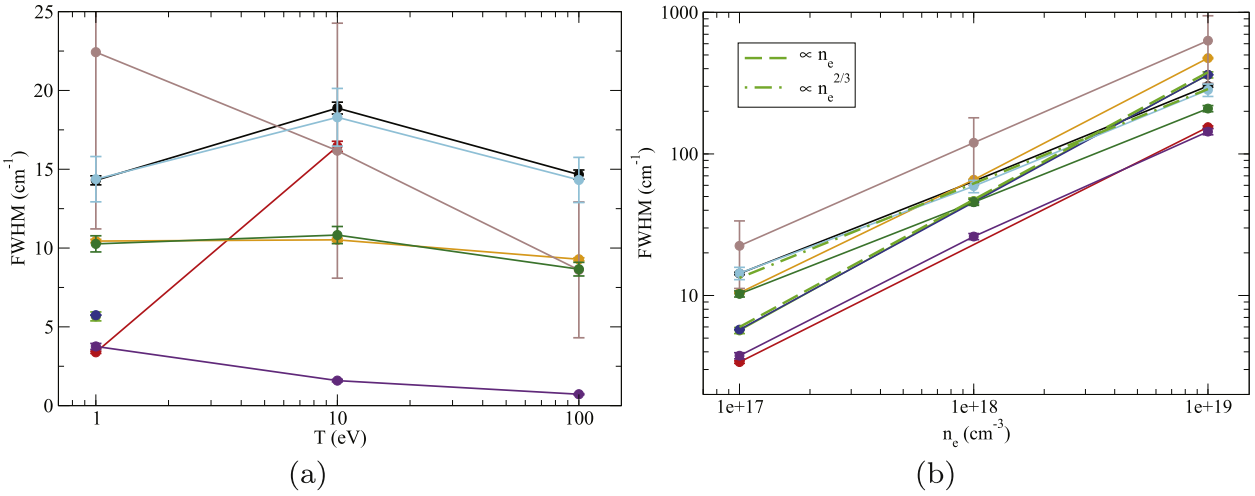


**Fig. 3.** Ly-$\alpha$ stark FWHMs as a function of (a) $T$ at a fixed $n_e = 10^{17}$ cm$^{-3}$ and (b) $n_e$ at a fixed $T = 1$ eV. Ideal two-component plasma consisting of electrons and protons is assumed.

respectively). Such transitions in H-like species have a strong unshifted component and are most influenced by the ion dynamics effect. This suggests that a major source of disagreement in these cases is an incomplete accounting for this effect. And indeed, an analysis presented in a separate study [15] confirms this.

One of the goals of the workshop was to check how the accuracy assessments are done. For a "consumer" of line-broadening calculations, knowledge of a *reliable* estimate of a result uncertainty is often not less important than the result itself. Therefore, we would like to draw the reader's attention to the error bars in Fig. 3. These reflect the uncertainties of the calculated values as claimed by the contributors.[1] Ideally, the error bars of all results for given plasma conditions should overlap, however, this is clearly not the case with the Ly-$\alpha$ results.

As can be gleaned from Fig. 2, the agreement between Ly-$\delta$ FWHM results for different codes is significantly better than those for Ly-$\alpha$. Although FWHM is often the most important characteristic of a line shape, in certain cases line wings is of significant practical interest, too. For example, at $n_e = 10^{18}$ cm$^{-3}$ and $T = 10$ eV, the maximal disagreement between different results is only about 20% in FWHM. However, the far wings of the line for the same conditions can still be challenging to get right, as Fig. 4 demonstrates. In addition to numerical issues associated with accurate calculations of values of the order of $10^{-3}$ of the line peak, the real physical phenomenon is a gradual transition of the electron broadening from the impact to quasistatic regime. Not unlike the ion dynamics effect, different codes approach this differently.

Let us consider next the isolated lines of the $3s$–$3p$ Li-like isoelectronic sequence (cases 4–6). The results are presented in Fig. 5. Among the three species (Be II, N V, and Ne VIII), the largest spread between different calculations is observed for the lowest $Z$ (Be II). This is rather surprising, because the interactions between the radiator and electrons are weakest for this ion – recall that the atomic model, $3s$, $3p$, and $3d$ level energies and matrix elements between them, was strictly defined and employed by all calculations. Another surprising observation is the growth of the relative spread between different results from ≈1.5–2 at 5 eV to ≈2–5 at 50 eV. Higher temperatures and/or lower $Z$ of the radiator

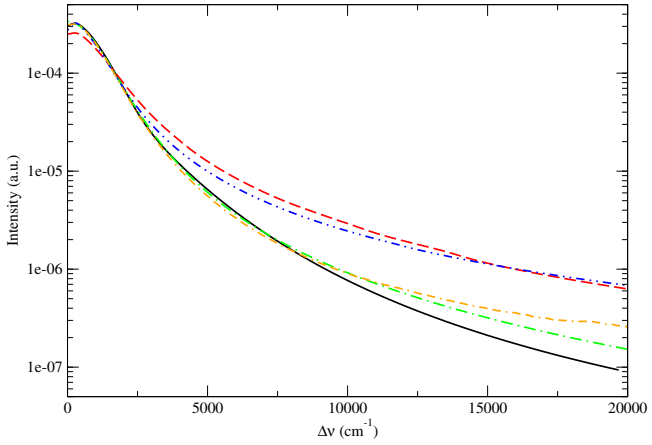


**Fig. 4.** Ly-$\delta$ Stark profiles at $n_e = 10^{18}$ cm$^{-3}$ and $T = 10$ eV. Ideal two-component plasma consisting of electrons and protons is assumed. While the FWHM values of different calculations agree within ≈20%, the intensities of the far wings differ by almost an order of magnitude.

correspond to smaller ratios between the electron-radiator potential energy and the kinetic energy of the electron, thus making the quasi-classical treatment of the electron scattering more justified.

The influence of the radiator–perturber interactions (RPI) on the line widths was investigated for these isolated lines, and results are given in Fig. 6. In the figure we plot relative corrections due to the RPI, calculated as

$$\frac{w_{\mathrm{RPI}} - w_{\mathrm{noRPI}}}{w_{\mathrm{RPI}}}, \tag{6}$$

where $w_{\mathrm{RPI}}$ and $w_{\mathrm{noRPI}}$ are FWHM with and without the RPI, respectively.[2] Based on these results, it is rather difficult to draw a general conclusion. One code predicts that the importance of the RPI diminishes for higher $T$, another one shows an increase of the opposite sign, while the results of the third one show a steep decrease from 5 eV to ≈15–25 eV and then an increase but of the opposite sign toward higher $T$.

[1] It should be stressed, that these uncertainties refer to inaccuracies inherent to the calculation methods *within the assumptions of the model(s) prescribed to a given case*. For example, a plasma with $n_e = 10^{17}$ cm$^{-3}$ and $T = 1$ eV is rather strongly coupled in reality, whereas the case-1 definitions postulated an ideal plasma.

[2] Since not all codes were able to switch the RPI without breaking some inherent assumptions, the number of results in this figure is less than in Fig. 5.

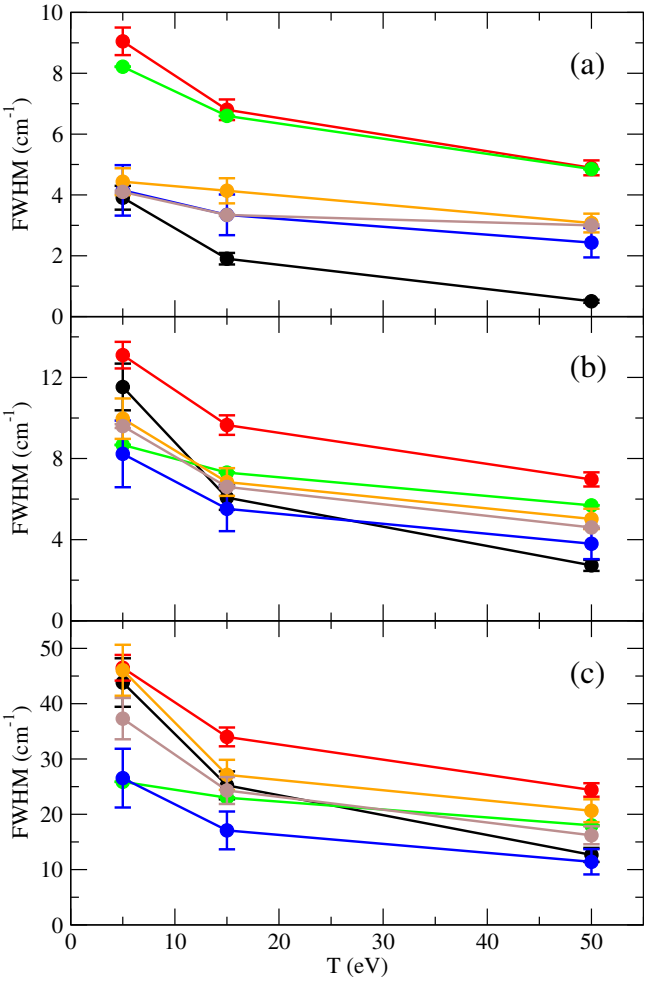


**Fig. 5.** Stark broadening of the 3*s*–3*p* transitions of three species from the Li isoelectronic sequence: (a) Be II at $n_e = 10^{16}$ cm$^{-3}$, (b) N V at $n_e = 10^{17}$ cm$^{-3}$, and (c) Ne VIII at $n_e = 10^{18}$ cm$^{-3}$.

The analysis of the micro-field correlations and their effect on line shapes (cases 13 and 14) showed a very good agreement between all submitted results and the results published previously [9,10]. Good agreement was also observed for the Stark broadening in the presence of a static magnetic field (cases 10 and 11). The same, however, cannot be said about the external periodic electric fields (case 9). Unfortunately, a very low number of submissions for this case make a meaningful comparison impossible. The results of case 15 will be published in a separate study [16], as will likely be others not discussed here.

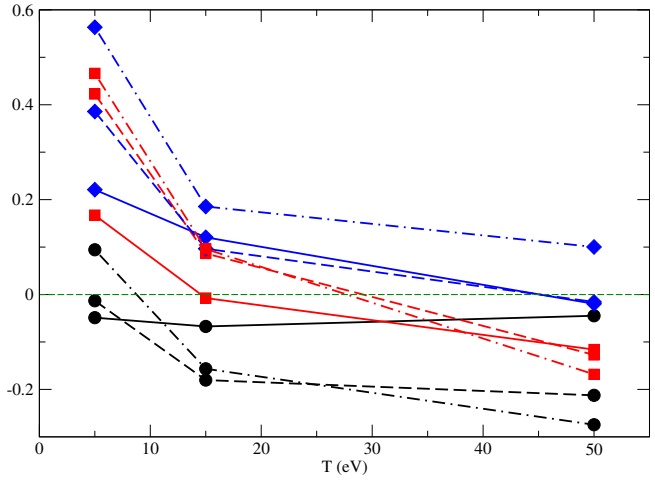


**Fig. 6.** The relative effect of the accounting for the RPI (6) on the Stark broadening of the 3*s*–3*p* transitions of Be II (solid lines), N V (dashed lines), and Ne VIII (dot-dashed lines). Different symbols correspond to different codes.

## 5. Conclusions

The SLSP workshop has been of great benefit to the participants and to the advance of the subject as a whole. A number of problems were identified, with a call for improvements made to achieve a better agreement between different calculations. In addition to this general review, two focused studies inspired by the workshop appear in *High Energy Density Physics* [15,16], with a few more in preparation.

A large number of test cases were selected, covering such diverse topics as transitions in hydrogen-like atomic systems, isolated lines, and intermediate cases; line shapes in the presence of external magnetic and electric fields; microfield correlation effects, and more. The extensive coverage also had a downside, resulting in too few results submitted for some cases. For the next workshop, a narrower selection of topics is planned. The 2nd SLSP workshop will be held from August 5 to 9 2013, and again be in Vienna.

## Acknowledgments

The workshop was realized and became possible due to a very large amount of work done by all participants. The organizational and financial support from the International Atomic Energy Agency (B.J. Braams and H.-K. Chung) is highly appreciated.

## References

[1] H.R. Griem, Principles of Plasma Spectroscopy, Cambridge University Press, 1997, ISBN 0 521 45504 9.
[2] Spectral Line Shapes in Plasmas code comparison workshop, http://plasma-gate.weizmann.ac.il/slsp/.
[3] R.W. Lee, J. Nash, Y. Ralchenko, Review of the NLTE kinetics code workshop, J. Quant. Spectrosc. Radiat. Transf. 58 (4–6) (1997) 737–742, http://dx.doi.org/10.1016/S0022-4073(97)00079-4.
[4] H.-K. Chung, C. Bowen, C.J. Fontes, S.B. Hansen, Y. Ralchenko, 7th Non-LTE Code Comparison Workshop: cases and lessons, High Energy Density Phys. (2013). in this volume.
[5] S. Rose, A review of Opacity workshops, J. Quant. Spectrosc. Radiat. Transf. 51 (1–2) (1994) 317–318, http://dx.doi.org/10.1016/0022-4073(94)90093-0.
[6] Y.V. Ralchenko, H.R. Griem, I. Bray, Electron-impact broadening of the 3s–3p lines in low-*Z* Li-like ions, J. Quant. Spectrosc. Radiat. Transf. 81 (2003) 371–384, http://dx.doi.org/10.1016/S0022-4073(03)00088-8.
[7] A.Y. Pigarov, J.L. Terry, B. Lipschultz, Study of the discrete-to-continuum transition in a Balmer spectrum from Alcator C-Mod divertor plasmas, Plasma Phys. Control. Fusion 40 (1998) 2055–2072.
[8] P. Tremblay, P. Bergeron, Spectroscopic analysis of DA white dwarfs: stark broadening of hydrogen lines including nonideal effects, Astrophys. J. 696 (2) (2009) 1755–1770, http://dx.doi.org/10.1088/0004-637X/696/2/1755.
[9] A. Calisti, B. Talin, S. Ferri, C. Mossé, V. Lisitsa, L. Bureyeva, M.A. Gigosos, M.Á. González, T. del Río Gaztelurrutia, J.W. Dufty, Electric micro fields in simulated two component plasmas, in: M.A. Gigosos, M.Á. González (Eds.), Spectral Line Shapes: Volume 15 19th International Conference on Spectral Line Shapes, vol. 1058, AIP, Valladolid, Spain, 2008, pp. 27–33, http://dx.doi.org/10.1063/1.3026461.
[10] E. Stambulchik, D.V. Fisher, Y. Maron, H.R. Griem, S. Alexiou, Correlation effects and their influence on line broadening in plasmas: application to $H_\alpha$, High Energy Density Phys. 3 (2007) 272–277 http://dx.doi.org/10.1016/j.hedp.2007.02.021.
[11] I. Golovkin, R. Mancini, High-order satellites and plasma gradients effects on the Ar He$_\beta$ line opacity and intensity distribution, J. Quant. Spectrosc. Radiat. Transf. 65 (1–3) (2000) 273–286, http://dx.doi.org/10.1016/S0022-4073(99)00073-4.

[12] E. Stambulchik, Y. Maron, Plasma line broadening and computer simulations: a mini-review, High Energy Density Phys. 6 (1) (2010) 9–14, http://dx.doi.org/10.1016/j.hedp.2009.07.001.
[13] Firefox; the free, non-profit browser for desktop and mobile, http://www.mozilla.org/firefox/.
[14] H.R. Griem, Spectral Line Broadening by Plasmas, Academic Press, New York, 1974, ISBN 0-12-302850-7.
[15] S. Ferri, A. Calisti, C. Mossé, B. Talin, S. Alexiou, M.A. Gigosos, M.Á. González, C.A. Iglesias, R.C. Mancini, E. Stambulchik, Ion dynamics effect on Stark broadened line shapes: a cross comparison of various models, High Energy Density Phys. (2013). in this volume.
[16] R.C. Mancini, C.A. Iglesias, S. Ferri, A. Calisti, C. Mossé, B. Talin, R. Florido, The effect of improved satellite line shapes on the Ar He$\beta$ spectral feature, High Energy Density Phys. (2013). in this volume.